

Beryllium and lithium X-ray lenses at the APS

Ali Khounsary^{ab}, Eric M. Dufresne^a, Kristina Young^{ab}, Cameron M. Kewish^a,
and Andrew N. Jansen^c

^aX-ray Science Division, Argonne National Laboratory, Argonne, IL 60439

^bDepartment of Mechanical, Materials, and Aerospace Engineering,
Illinois Institute of Technology, Chicago, IL 60616

^bChemical Engineering Division, Argonne National Laboratory, Argonne, IL 60439

ABSTRACT

Compound refractive lenses (CRLs) are arrays of concave lenslets used to focus X-rays. For a given incident X-ray beam energy, the focal length of a CRL depends on the material and shape of the individual lenslets, and in particular is inversely related to the number of lenslets in the array. The throughput of a lens array is heavily affected by absorption of the X-rays in the lens. For this reason, it is necessary to employ low-atomic-number materials and fabricate the lenses as thin as possible, especially for low to moderate X-ray energy range (~ 5 - 20 keV) photons.

Lithium and beryllium are two of the best candidate materials for X-ray lenses due to their relatively high (real decrement) index of refraction and low X-ray absorption. Lithium is very malleable, however, and reacts strongly with moisture in the air, requiring a special fabrication environment and housing. Beryllium, on the other hand, is a solid metal and is easy to machine and handle.

This paper summarizes the recent work at the Advanced Photon Source (APS) on parabolic lithium and cylindrical beryllium lenses. These lenses have been tested on APS X-ray beamlines. Their performance in terms of the focal size and gain is described and further improvements including tighter manufacturing tolerances and thinner lens walls are discussed.

Keywords: focusing, X-ray lens, compound refractive lens, CRL, lithium, beryllium, gain

1. INTRODUCTION

Nanometer-sized X-ray beams are in increasing demand for a variety of scientific and technical applications [1-4]. They are produced by focusing X-ray beams using a variety of techniques. By virtue of their size (approaching about 1 nm), they provide information with high spatial resolution, and due to the high intensity resulting from focusing, they allow high sensitivity in a multitude of X-ray techniques and applications. In addition, the developments in this field are naturally of interest in nanosciences and nanotechnology.

There are a number of techniques to focus X-rays, using, for example, mirrors, crystals, capillaries, waveguides, zone plates, and lenses. The choice depends on the desired focused beam size, energy, bandwidth, intensity, etc. X-ray lenses, first developed by Snigirev in 1996 [5] have simple designs and a wide range of applications. They are cost effective, relatively insensitive to figure and finish imperfections, and are easy to install and use (usually used in air on a motorized stage). An X-ray lens is composed of one or more thin concave lenslets lined up and arranged in an array to focus an incident X-ray beam. The focal distance f for an X-ray lens is given in the thin lens limit as:

$$f = \frac{R}{2N\delta}, \quad (1)$$

where R is the lenslet radius, N is the number of lenslets (typically 10-100), and δ is the real index of refraction decrement. To a first approximation (ignoring the diffraction limit), the width of the focal spot is obtained by dividing

the source width by the demagnification factor M , while the gain is simply M^2T , where transmission T accounts for absorption in the lenslet walls.

To minimize absorption of X-rays, lens materials should be comprised of lighter elements. Li, Be, Al, Is, PMMA, Mylar, Ni, and similar low-atomic number materials have been used [5-15]. A figure of merit in this context is the ratio δ/β , where β is the material absorption coefficient. Of all solids considered, LiH has the highest figure of merit, followed by Li, and Be. Lithium is soft, malleable, and reacts strongly with moisture and water. As such, Li lenses must be fabricated in a dry environment or in vacuum. Furthermore, Li adheres to tools in contact with it, resulting in poor lenslet surface characteristics. Beryllium, on the other hand, is highly machinable and can be polished if needed; yet it is a hazardous material requiring safety measures during fabrication. For this reason, Be work is carried out by specialized vendors.

In this paper, we report on our recent work on lithium [16] and beryllium [17] lenses; briefly describe their fabrication, testing, and performance; and point out plans for next generation lenses.

2. LITHIUM LENS

Lithium lenslets are fabricated from thin lithium foils (Fig. 1-a). Ten-mm-diameter disks are punched out of a foil (Fig. 1-b), and each placed securely in a holding cartridge having two alignment holes (Fig. 1-c). Using two parabolic indenters (Fig. 1-d) mounted in a precision manual press (Fig. 1-e), the cartridge, now positioned and aligned in the press, is indented to produce the desired profile on both sides. Once all the lenslets are made, the cartridges are assembled and aligned as shown in Fig. 1-f. This assembly is then placed in a sealed housing mounted on the experimental table as shown in Fig. 1-g. The housing has two Be windows on each side to allow X-rays to pass. This process is performed in a dry room.

A lens to focus 10-keV photons was designed and fabricated. The desired focal length was 1-2 m. Parabolic indenters made of stainless steel with tip radii of 100 μm were fabricated and used to press the lenslets. The optical aperture of the lenslets is about 0.5 mm. Thirty-two (32) lenslets were made and assembled, for an expected focal length of 1.7 m (see Eq. (1)). Lens specifications are summarized in Table 1. The lens was tested on APS beamline 7-ID, where the source-to-lens distance is about 50 m, resulting in an expected demagnification of about 29. The focus is measured using a CCD camera mounted on a slide [14]. The camera moves back and forth measuring the focal size in an attempt to establish the smallest image size at the focus. The goal of the experiment was to measure the location and size of the focus, lens transmission, and lens gain.

Table 1: Specifications of the lenses

Specification	Lens	
	Lithium foil	High Purity Beryllium
Material	Lithium foil	High Purity Beryllium
Lenslet shape	Paraboloid	Cylindrical
Focusing	2-D	1-D
Lenslet tip radius (mm)	0.1	0.5
Lens aperture (mm)	0.5	<1.0
Desired focal length (m)	1-2	1-2
Number of lenslets	32	10, 20, 30, 40, 50
Wall thickness (μm)	100	100
RMS Roughness (μm)	~ 0.5	~ 0.1
Fabrication method	Precision press	CNC

Figure 2 shows the vertical and horizontal size (FWHM) of the image at various distances from the lens. Focal distance and focus size are hence determined. Figure 2 shows the FWHM focal size to be 34 μm horizontally and 24

μm vertically. Figure 3 shows the beam at focus with and without the lens. Table 2 summarizes the experimental results.

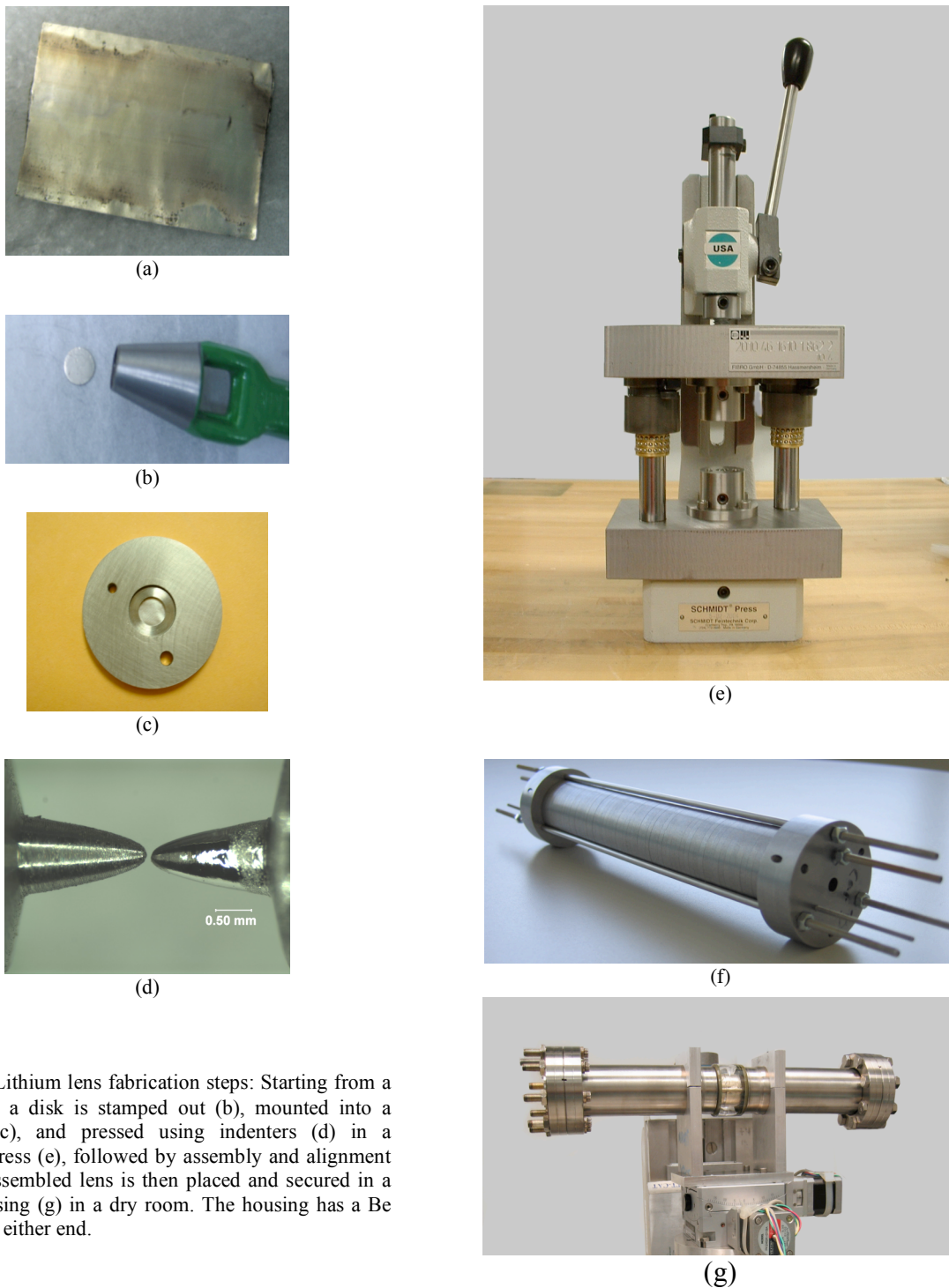


Figure 1: Lithium lens fabrication steps: Starting from a Li foil (a), a disk is stamped out (b), mounted into a cartridge (c), and pressed using indenters (d) in a precision press (e), followed by assembly and alignment (f). The assembled lens is then placed and secured in a sealed housing (g) in a dry room. The housing has a Be window on either end.

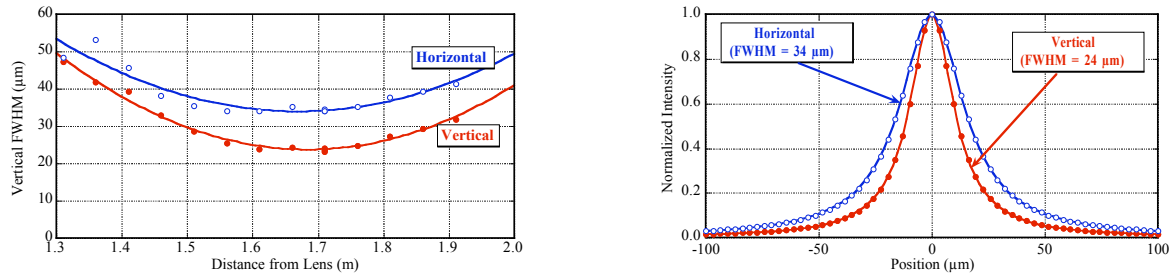


Figure 2: Vertical and horizontal FWHM of the beam along the optical axis is obtained to determine focal distance (left). The profiles at focus are shown on the right.

By comparing the horizontal and vertical sizes of the focal spot, and assuming that lenslet surface imperfections broaden the focal spot by a similar amount (in quadratures), we can estimate this contribution to be about 24 μm . Hence, there is a need to improve the lenslet production procedure.

Attempts were made to estimate the roughness and profile of the produced Li lenslets. This was challenging because the Li must be kept in dry air, but metrology instruments are kept in a clean but not dry environment. We tried replicating the lens surface using a polymer poured into the concave lenslet. Upon curing the polymer was removed and its surface measured in the metrology lab. We obtained limited information from this, but feel that the process can be improved to obtain better data.

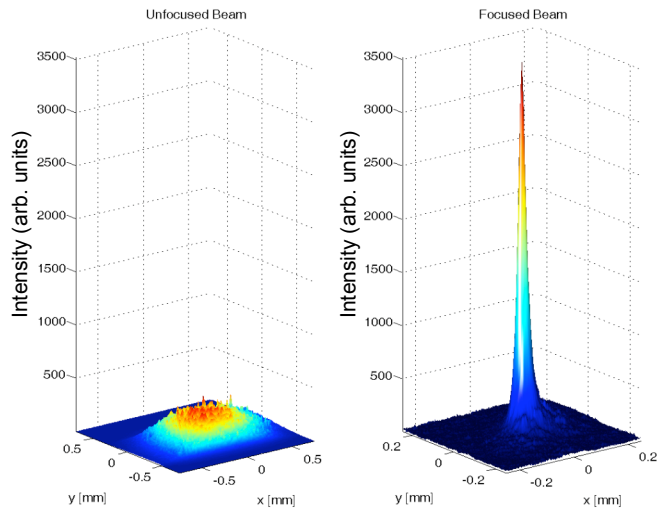


Figure 3: Profile of the unfocused (left) and focused (right) beam at focus.

Table 2: Expected and measured performance of the Li and Be lenses

Lens / Focusing	Lithium / 2-D		Beryllium / 1-D	
	10 keV		11 keV	
Energy	Expected	Measured	Expected	Measured
Transmission (%)	85	~ 85	43	43
Focal Distance (m)	1.70	~ 1.71	1.77	1.73
Focal size (μm)	0.7(v) x 22(h)	24(v) x 34(h)	0.7(v)	2.3(v)
Gain	~ 800	~ 18	58	19

3. BERYLLIUM LENS

Beryllium lenses were fabricated by precision drilling holes, 1 mm diameter and 5 mm deep, into a 10-mm-thick beryllium substrate. A total of about 150 holes (lenslets) were drilled into a single block, which was subsequently cut to produce lenses with 10, 20, 30, 40, and 50 lenslets. One such lens is shown in Fig. 4. Each lens is used alone or in tandem with others to provide a wide range of foci. The specified surface roughness is 0.4 μm rms, but measurements show a wall roughness of about 0.1 μm rms.

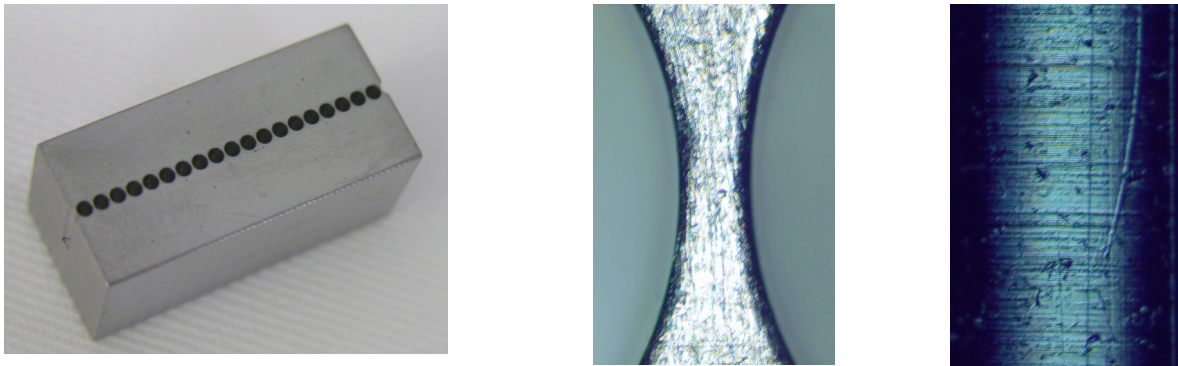


Figure 4: A beryllium lens with 20 lenslets in a 20 mm x 10 mm x 10 mm substrate (left). The lenslets are 5 mm deep. Closeup pictures of a lenslet and its wall surface structure are shown in the center and right, respectively.

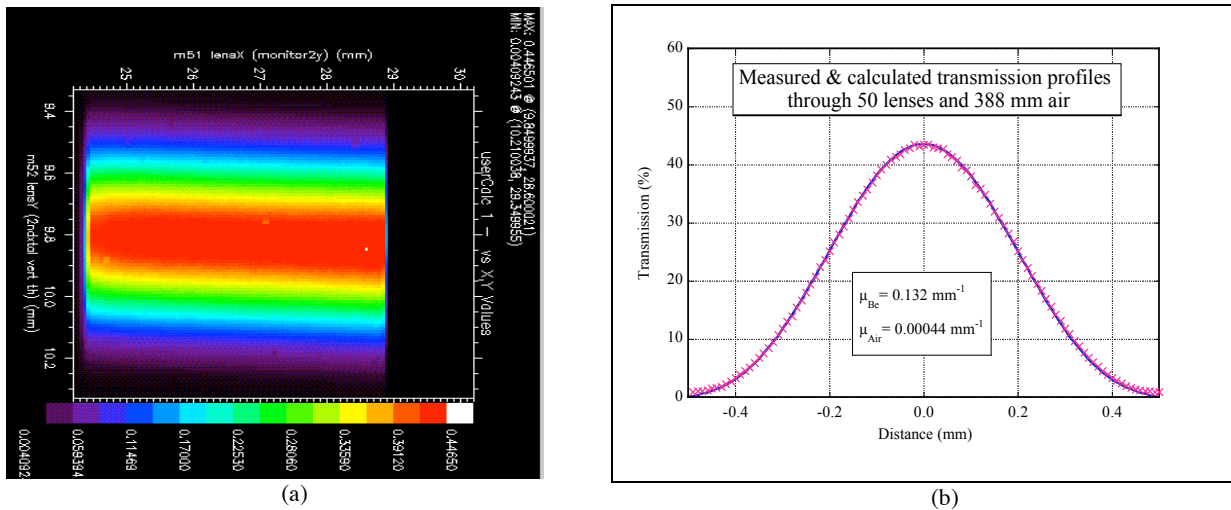


Figure 5: (a) Intensity profile of X-rays transmitted through the lens was obtained by scanning the lens through a $30 \mu\text{m}$ by $10 \mu\text{m}$ beam. The legend displays the ratio $IC1/IC0$ uncorrected for attenuation in air. (b) A cut across the image after correcting for the attenuation in air. A good fit was obtained, indicating an absorption coefficient of 0.132 mm^{-1} .

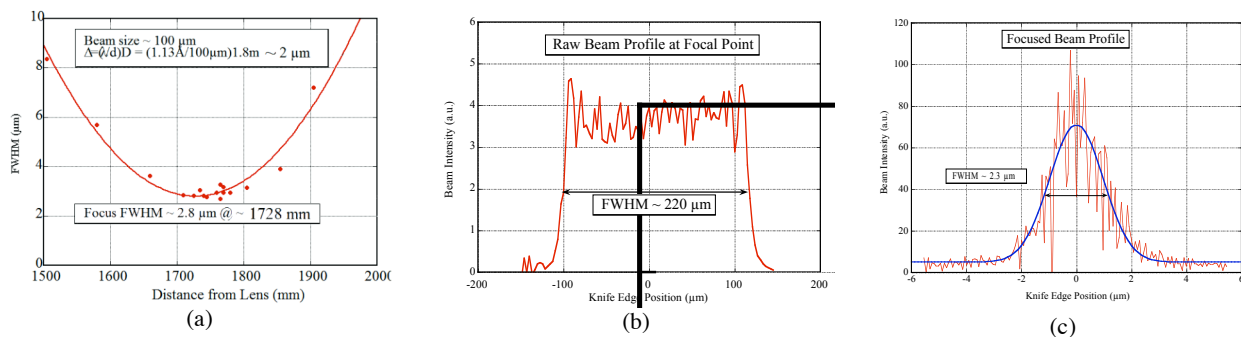


Figure 6: Vertical FWHM of the beam along the optical axis is measured to determine focal distance (a). The vertical profiles of the beam at focus without (b) and with (c) the lens are shown. The lens is 49.8 m from the source. The source vertical size is $20 \mu\text{m}$.

A Be compound refractive lens with 50 lenslets was also tested on beamline 7-ID of the APS using a slightly different procedure. For this experiment, a white beam with its fundamental energy set at 11.0 keV was collimated with a

0.5 mm x 0.5 mm slit placed 26.5 m from the Undulator A source. A double-crystal Si(111) monochromator, placed 30 m from the source, diffracted 11.0-keV X-rays with an energy band pass of $\Delta E/E = 1.4 \times 10^{-4}$. The monochromator was detuned to minimize 3rd harmonic contamination, reducing the 11.0-keV flux by 25%. An aperture to reduce the beam size was placed 462 mm upstream of the lens center. The vertical opening was varied from 10-800 microns, but the horizontal size was set at 50 microns. Three ion chambers (IC) were used to record the X-ray signal; we denote these as IC0 just after the slit and before the lens, IC1 after the lens, and IC2 downstream well beyond the focal point. A knife edge was scanned vertically with a stepper-motor-controlled stage in the focal plane, and the ratio of IC2/IC1 was used to measure the focal plane intensity profile. This knife edge could also be positioned along the optical axis of the lens with a motorized stage to measure the depth of focus.

Figure 5-a shows the transmission profile of the lens. The profile is quite smooth over the length and width of the hole and the transmission drops to zero at the top and bottom when the beam hits the mount of the lens. Figure 5-b shows a cut through Fig. 5-a. A fit to the calculated X-ray path corrected for air paths around the lens is shown and agrees quite well with the data. The peak transmission is 43% as expected for Be with an absorption coefficient of 0.132 mm^{-1} .

Figure 6-a shows the downstream beam FWHM as a function of distance from the lens, and also shows the lens depth of focus. In this part of the experiment the beam size in front of the lens was set to $100 \text{ }\mu\text{m}$, for which the diffraction-limited focal spot size is about $2 \text{ }\mu\text{m}$ at 11 keV (wavelength of 0.113 nm). A quadratic fit to the data is shown as a solid line. The best focus from the fit is $2.8 \text{ }\mu\text{m}$, located 1.728 m from the lens center. From the thin lens formula and the focal length formula (Eq. 1), one expects the lens-to-image distance $S_i = 1.77 \text{ m}$. This small difference may be due to deviation in lenslet radius and difference between the measured and calculated index of refraction decrement of Be.

The slit in front of the lens was then widened to $250 \text{ }\mu\text{m}$. Figure 6-b shows the raw beam profile in the plane of the focus with the lens out of the X-ray beam path. The derivative of the ratio of IC2/IC1 versus knife-edge position is shown. Fresnel fringes are clearly seen from the edges of the beam profile. The FWHM of the unfocused beam is $220 \text{ }\mu\text{m}$. Figure 6-c shows the focused beam in the same intensity units as Fig. 6-b. From the peak intensity difference between these two figures, the gain is about $70 / 3.9 = 18$. There is a notable background intensity in Fig. 6-c, where the ratio of peak to background intensity is $70 / 5 = 14$. Although not shown, we have found this ratio decreases as the slit opening is increased. We attribute this background to lens aberrations. The FWHM of the focused beam is $2.3 \text{ }\mu\text{m}$. The diffraction-limited focal spot FWHM is calculated as $\lambda S_i / D \approx 0.113 \text{ nm} \times 1.73 \text{ m} / 250 \text{ }\mu\text{m} = 0.78 \text{ }\mu\text{m}$. The demagnified FWHM source size is $20 \text{ }\mu\text{m} \times 1.73 \text{ m} / 49.8 \text{ m} = 0.69 \text{ }\mu\text{m}$. Convoluting the two effects in quadrature, we expect a focal spot FWHM of $1.04 \text{ }\mu\text{m}$. Integrating Fig. 6-c, we find a total measured transmission of 24%. We estimate the gain from $(\text{slit width})/(\text{ideal focal spot}) \times T = 250 \text{ }\mu\text{m} / 1.04 \text{ }\mu\text{m} \times 24\% = 58$.

We obtained a gain of approximately 19. The difference is probably due to a few factors such as spherical aberration, error in best focal plane location, and lens imperfections. In addition, a 0.5-mm-thick GaAs knife edge was used to obtain the intensity profile; a slight misalignment of this edge to the beam may cause additional blurring.

4. NUMERICAL MODELING

The focal length and the size of the focal spot produced by a lens can be estimated from the thin lens equation and the demagnification factor, respectively. However, as seen, imperfections in the X-ray lens can considerably broaden the focus, and a procedure to compute the contributions from various sources is very helpful. Broadening due to deviations in shape, size, alignment, as well as surface roughness could then be estimated.

For this purpose, a new computer program has been developed with the objective of simulating the focusing performance of X-ray refractive lenses. The program utilizes wave optical calculations to obtain the complex wavefield amplitude downstream of a lens illuminated (for now) by monochromatic radiation. The simulation geometry consists of monochromatic plane waves normally incident upon a concave lens (see Fig. 7).

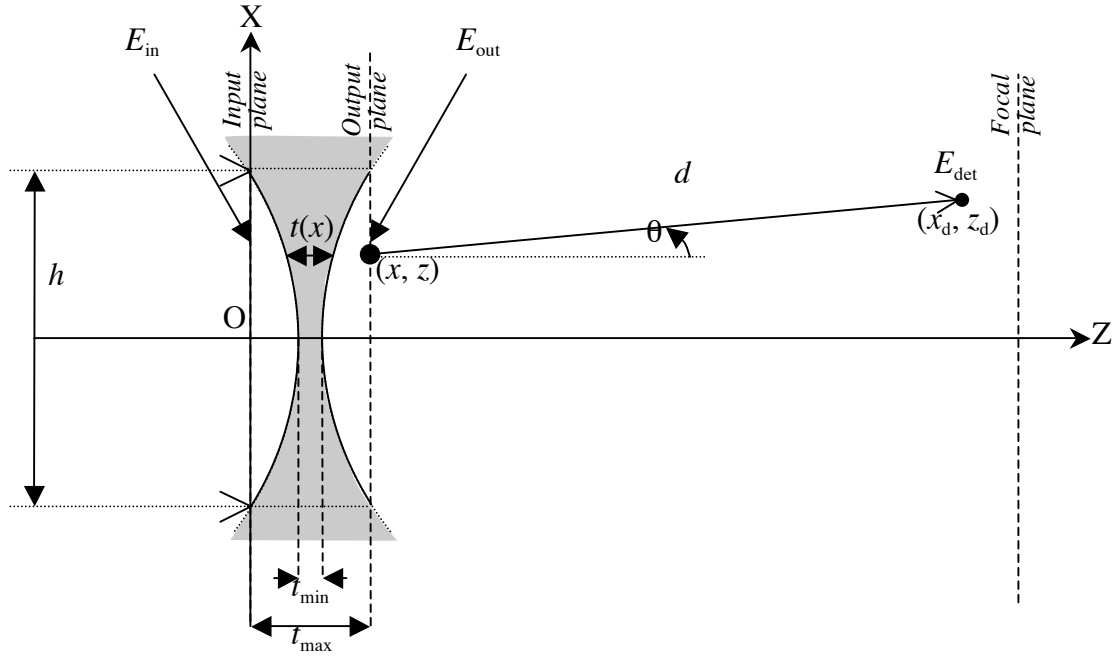


Figure 7: Simulation geometry (for focusing in one dimension) for modeling the refraction of X-rays by a single concave cylindrical lens. The thickness of the lens $t(x)$ traversed by the radiation varies as a function of distance x from the optical axis, from $t(0) = t_{\min}$ at the center of the lens to $t(h/2) = t_{\max}$ at the edge of the illuminated region. The incident plane wave amplitude E_{in} , the refracted wave amplitude E_{out} , and the amplitude E_{det} detected at a distance d from the output plane are shown. The lens is continuous along the y -axis (into the page), so the geometry is shown for two dimensions as a slice along the x - z plane.

Each lens is modeled as a region with a complex refractive index $n = 1 - \delta + i\beta$ in which the real and imaginary components are δ and β respectively. The thickness of the lens $t(x) = t_1(x) + t_{\min}$ varies with distance x from the optical axis z . The precise format of $t_1(x)$ is dependent on the shape of the lens.

The formulation assumes that a collimated plane wave of wavelength λ is incident on the first lens, and the field E_{in} is constant over the input plane perpendicular to the optical axis (see Fig. 7). The output wavefield transmitted by a compound lens consisting of N lenslets (identical or otherwise) is obtained by calculating the phase delay experienced by the wave due to the complex refractive index of a lens. Both refraction and absorption within the lens material as well as the phase advance of the wave propagating between the lenslets are accounted for.

To obtain the wavefield downstream of the lens, the output wavefield is treated as an ensemble of secondary (Huygens') wavelets, and the complex amplitude propagated to the detection point is integrated over the whole output wavefield. Since the extreme rapidity of wavefield oscillations precludes the measurement of the phase in an experiment, we calculate the intensity at the detection point as the time-averaged square magnitude of the complex amplitude.

As an example, the intensity distribution downstream of the Be lens tested (with 50 identical lenslets) is obtained. The calculation is repeated for a parabolic lens as well. A monochromatic plane wave, 0.5 mm high, with a wavelength of $\lambda = 1.127 \text{ \AA}$ (corresponding to $E = 11 \text{ keV}$) incident on the lens is assumed.

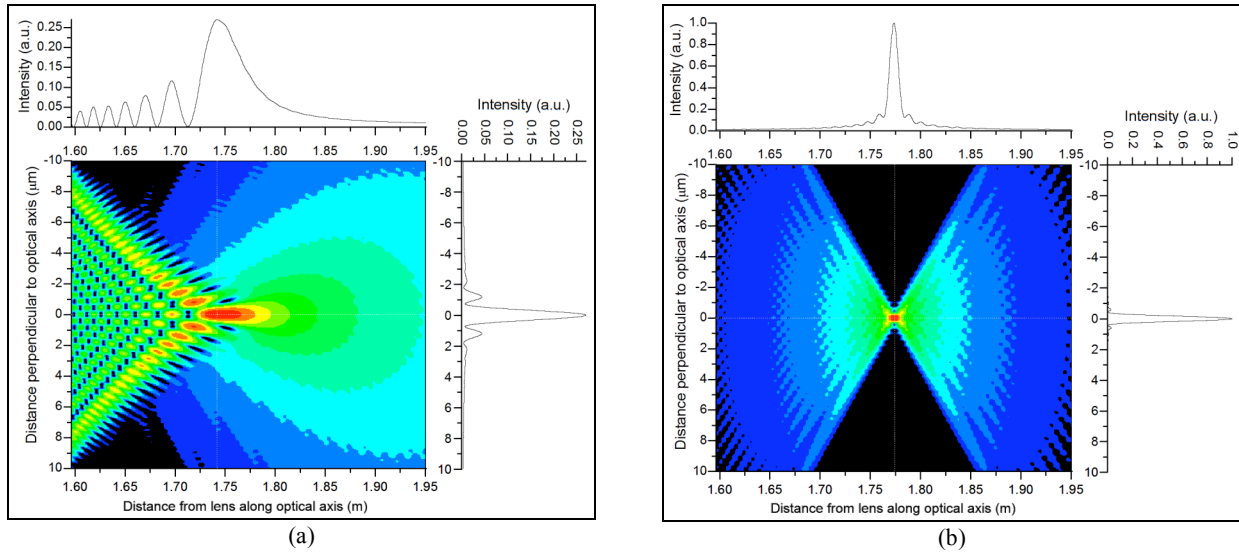


Figure 8: Isophotes in the x - z plane (along the optical axis) simulated for a collimated plane wave incident on a compound refractive lens consisting of $N=50$ identical cylindrical (left) and parabolic (right) Be lenslets. The line profiles adjacent to the isophotes diagrams indicate the intensity in the focal plane (perpendicular to the optical axis) and along the optical axis. Evidence of spherical aberration is seen in the left figure with calculated focal length of 1.74 m and a FWHM focal spot size of 0.69 μm . For the parabolic profile lens, these numbers are 1.7736 m and 0.37 μm , respectively. The focal spot of the parabolic lens is almost four times more intense at the peak than the cylindrical lens.

From the thin lens equation and Eq. (1), the approximate geometrical focal distance for 50 thin lenses is 1.77 m. Calculated results shown in Fig. 8-a show that for the cylindrical lens, the focal spot is located 1.74 m downstream of the lens and has a FWHM of 0.69 μm . Significant spherical aberration is seen, as the focal spot is broadened both laterally and along the optical axis, significantly reducing the peak intensity (by almost a factor of 4). The parabolic lens (Fig. 8-b), on the other hand, has a symmetrical focus located at 1.77 m as predicted, and a focal spot FWHM size of 0.37 μm with an estimated depth of field of about 60 mm (focusing tolerance).

The simulation program is being further developed to calculate the effects of lenslet surface figure and finish imperfections. These all modify the phase of the transmitted wave by introducing variations in the optical path length through the lens system. Other geometrical misalignments, including displacement of lenses from the optical axis and relative angular inclinations of the lenses, are anticipated to provide unique insights into the mechanical tolerances permissible in the fabrication and implementation of compound refractive lenses for synchrotron beamlines.

5. CONCLUSIONS

Recent work on the fabrication of a lithium lens with paraboloidal profile (for 2-D focusing) and a beryllium lens with cylindrical (for 1-D focusing) is reported. We have been able to obtain 24 μm FWHM focal size with Li lenses and 2.5 μm with Be lenses. While the measured focal distance and X-ray transmission of the lenses are close to theoretical predictions, the focal spot size and gain are not. Qualitative study of the fabricated lens shape and surfaces indicate that the broadened focal spot and reduced gain are the results of imperfections in the lenslets, more so for Li than Be. Our plan is to improve the fabrication processes for both types of lenses to better control surface imperfections. For lithium, it is necessary to better understand its mechanical behavior (spring back, flow, adhesion), improve the shape and roughness of the paraboloidal stainless steel indenters, reduce tip radius below 100 μm , and develop the means to characterize surfaces in a dry environment. For Be lenses, the plan is to produce more precise and smoother lenslets with thinner walls to reduce X-ray absorption by Be. In addition, further development of the wavefield calculations will allow us to model lens imperfections and quantify their effects on lens performance.

6. ACKNOWLEDGEMENTS

The authors wish to acknowledge contributions to this work made by, J.-I. Yum, L. Assoufid, Q. Jun, A. Macrander, J. Cremer, and N. Pereira. This work is supported in part by the U.S. Department of Energy, Office of Science, Office of Basic Energy Sciences, under Contract No. W-31-109-ENG-38.

7. REFERENCES

1. G. E. Ice et al., *Compos. Sci. Tech.* 36, 271-277 (2005).
2. B. Lengeler et al., *App. Phys. Letters* 74 3924-3926 (1999).
3. C. G. Schroer et al., *Proc. SPIE*, Vol. 5535, 162-168 (2004).
4. C. G. Schroer et al., *Proc. SPIE*, Vol. 5535, 715-723 (2004).
5. A. Snigirev et al., *Nature* 384, 49-51 (1996).
6. M. A. Piestrup et al., *Rev. Sci. Instrum.* 71 4375-4379 (2000).
7. A. M. Khounsary et al., *Proc. SPIE*, Vol. 4783 (2002).
8. H. R. Beguiristain et al., *Optics Letters* 27, 778-780 (2002).
9. B. Lengeler et al. *Proc. SPIE*, Vol. 5539 (2004).
10. D. A. Arms et al., *Rev. Sci. Instrum.*, 73 1492-1494 (2002).
11. J. T. Cremer et al. *Rev. Sci. Instrum.*, 74 2262-2266 (2003).
12. N. R. Pereira et al., *Rev. Sci. Instrum.*, 75 37-41 (2004).
13. K. Young, A. Khounsary, *Proc. SPIE*, Vol. 5539, 31-37 (2004).
14. E. M. Dufresne et al., *AIP Conf. Proc.*, 705, 780 – 783 (2004).
15. B. Cederstrom et al., *Appl. Phys. Lett.* 81,1399-1401 (2002).
16. K. Young, et al., accepted for publications, SRI 2006, Korea, (2006).
17. A. Khounsary et al., presented at MEDSI 2006, Himeji, Japan, (2006).